Applied Catalysis B: Environmental 88 (2009) 497–504

Contents lists available at ScienceDirect

Applied Catalysis B: Environmental

journal homepage: www.elsevier.com/locate/apcatb

Photocatalytic mineralization of phenol catalyzed by pure and mixed phase hydrothermal titanium dioxide

Roberto Scotti *, Massimiliano D'Arienzo, Andrea Testino, Franca Morazzoni

INSTM, Department of Materials Science, University of Milano-Bicocca, Via R.Cozzi 53, I-20125 Milano, Italy

ARTICLE INFO

Article history:
Received 1 August 2008
Received in revised form 13 October 2008
Accepted 18 October 2008
Available online 6 November 2008

Keywords:
Electron paramagnetic resonance
Spin-trap
Hydroxyl radicals
Ti^{3+}
O^-
Rutile
Anatase
Photocatalysis

ABSTRACT

The photocatalytic mineralization of phenol catalyzed by pure (anatase, rutile) and mixed phase hydrothermal TiO_2 was studied in aqueous solution employing different oxidative agents, H_2O_2 and O_2. In the case of H_2O_2, rutile particles, having large dimensions and high aspect ratio (size: 30–70 nm × 150–350 nm), display the highest catalytic activity due to their low tendency to recombine electrons and holes generated by UV irradiation. By using water dissolved gaseous O_2, the catalytic TiO_2 activity generally decreases and rutile displays the lowest efficacy. In fact, oxygen preferentially chemisorbs at the surface of the nanosized particles of anatase (5–15 nm) and acts as effective electron scavenger, inhibiting the electron-hole recombination. The number of electron and hole traps (Ti^{3+}, O_2^- and O^-) and the rate of formation of the short-lived hydroxyl radicals $OH^\bullet$ under UV irradiation, were evaluated by electron paramagnetic resonance (EPR). A correlation was suggested among the amount of the charge carrier centers, the rate of formation of $OH^\bullet$ radicals and the catalyst photoactivity. This confirms that the photocatalytic properties depend on the possibility that electrons and holes separately interact with the oxidative agents at the TiO_2 surface, inducing the formation of $OH^\bullet$ radicals.

1. Introduction

For about 10 years there have been many reports in the literature about TiO_2, due to its promise in the photodegradation of organic pollutants in air or water at room temperature and pressure [1].

In spite of the large number of scientific contributions concerning TiO_2 with different crystalline phase, surface area, particle and pore size, the relationships between morphology, structural properties and the catalytic behavior need further investigations. In fact some authors suggested that anatase phase provides the highest photoactivity [2], others claimed at the synergistic effects on the photoactivity of anatase–rutile mixed phases [3], a few number indicated rutile as the best catalyst [4]. These contrasting results are often attributable to photodegradation reactions performed on different substrates and/or by different oxidative agents (e.g. oxygen, air, hydrogen peroxide). High surface area and mesoporous structures were also relevant to the photoactivity and many efforts were done in order to obtain TiO_2 with high and controlled porosity [5].

Several methods were suggested to prepare highly photoactive TiO_2, by varying crystalline phase, morphology, particle size and shape, porosity. Recently, we reported about synthesis, crystal structure and morphology properties of several TiO_2 samples with definite phase composition (rutile:anatase ratio), obtained by hydrothermal [6] and by template assisted sol-gel [7] methods. It was found that using H_2O_2 as oxidative agent, the photoactivity increases with the rutile content and pure rutile displays the highest catalytic efficiency. Instead using gaseous O_2 as heterogeneous oxidative agent, the highest photocatalytic activity is displayed by anatase and anatase-rich samples. The lower surface area and pore volume of rutile with respect to anatase, do not agree with the photocatalytic behavior, suggesting that the effects of the phase composition are dominant.

The charge trap centers (Ti^{3+}, O^-, O_2^-) of the UV-photogenerated electron e^- and hole h^+ pairs in TiO_2 were studied by electron paramagnetic resonance (EPR) spectroscopy. Their detection was assumed as a measure of the e^-–h^+ charge separation and, in turn, of the photocatalytic efficiency [7]. In fact, if e^- and h^+ do not recombine, the following processes can be assumed as reaction steps [8,9] either when the oxidant is H_2O_2 or O_2.

Photogenerated holes (h^+) can be trapped to lattice oxide ions giving O^- centers:

$$O^{2-} + h^+ \rightarrow O^- \quad (1)$$

* Corresponding author. Tel.: +39 02 64485123; fax: +39 02 64485400.
E-mail address: Roberto.Scotti@unimib.it (R. Scotti).

0926-3373/$ – see front matter © 2008 Elsevier B.V. All rights reserved.
doi:10.1016/j.apcatb.2008.10.017

or forming $OH^{\bullet}$ radicals, with high oxidizing potential (2.7 V in acidic solution; 1.8 V in neutral solution) [10]:

$$O^{2-} + h^{+} + H^{+} \rightarrow OH^{\bullet} \quad (2)$$

O^{-} and $OH^{\bullet}$ species react with the organic substrates, generating organic radicals [11]:

$$O^{-}/OH^{\bullet} + PhOH \rightarrow O^{2-}/OH^{-} + PhO^{\bullet} + H^{+} \quad (3)$$

further oxidized to intermediates compounds [12–14] until complete mineralization to CO_2 and H_2O.

Photogenerated conduction band electrons e^{-} may interact with the oxidant (H_2O_2 or O_2) according to the following reactions [8,9,15,16]:

$$H_2O_2 + e^{-} \rightarrow OH^{\bullet} + OH^{-} \quad (4)$$

$$O_2 + e^{-} \rightarrow O_2^{\bullet -} \quad (5)$$

$O_2^{\bullet -}$ centers may further generate H_2O_2 [8,17,18]:

$$O_2^{\bullet -} + H_2O \rightarrow HO_2^{\bullet} + OH^{-} \quad (6)$$

$$HO_2^{\bullet} + H_2O + e^{-} \rightarrow H_2O_2 + OH^{-} \quad (7)$$

$$H_2O_2 + O_2^{\bullet -} \rightarrow OH^{\bullet} + OH^{-} + O_2 \quad (8)$$

successively, $OH^{\bullet}$ radicals interact with phenol via reaction (3).

Basing on the above arguments and aiming to obtain deeper insight, at electronic level, into the photoactivity mechanism of TiO_2, it seemed to us helpful that TiO_2 catalytic behavior would be studied in relation not only to the crystalline phase, but also to the amount of charge trapping centers and of intermediate radical species $OH^{\bullet}$, active in the oxidation reaction. EPR spin-trapping investigation is a really good technique for detecting the short-lived radicals by formation of stable paramagnetic adducts [19,20].

The present paper reports about the phenol photomineralization in the presence of some selected hydrothermal TiO_2 samples with different phase composition, by using both H_2O_2 and O_2 as oxidizing agents in aqueous solution.

Photomineralization of phenol was followed by measuring the total organic carbon (TOC) at different reaction times. The decrease of the TOC amount during the reaction was related: to the type and the amount of charge trapping centers, Ti^{3+}, O^{-} and O_2^{-}, detected by EPR in irradiated solid catalysts; to the ease of formation of $OH^{\bullet}$ radicals, after UV irradiation of TiO_2 in the presence of the oxidant agent. Radicals were reacted with the spin-trap molecule α-(4-pyridil-1-oxide)-N-*tert*-butylnitrone (POBN) and the resulting adduct detected by EPR spectroscopy.

A correlation was suggested among the catalyst efficacy, the charge carrier amount and the ease of hydroxyl radical formation.

2. Experimental

2.1. Synthesis procedure

Hydrothermal synthesis of TiO_2 was performed according to the previously reported procedure [6] by reacting aqueous solutions of $TiOCl_2$ (0.45 mol kg^{-1}) with 0–50 ml of NH_3 solution (28.0 wt%) in a Teflon lined autoclave. The amount of water was that required to have an overall mass of 360 g for each experiment. Different amount of NH_3 was required to tune the crystalline phase composition [6]. The autoclave temperature was increased by 2.67 °C/min up to 30 °C and then by 0.75 °C/min up to 220 °C. At this temperature the suspension was aged for 2 h. After decantation, TiO_2 powder was recovered from the autoclave and washed with water, then with ammonia solution and finally with acetone. The powder was filtered and dried under vacuum at room temperature. Phase composition was determined by X-ray diffraction (XRD) patterns, collected with a Bruker D8 Advance diffractometer (Cu Kα radiation) in the range 20–40° 2θ (2θ step 0.020°, counting time 2 s per step). The diffraction peaks were indexed as pure rutile TiO_2 (JCPDS, no. 21-1276), and pure anatase (JCPDS, no. 21-1272).

Hereafter, TiO_2 samples were labelled as Rnn, where nn stand for the wt% of rutile phase as reported in Table 1.

2.2. Photoinduced degradation of phenol

Photodegradation experiments were carried out in a 400 ml pyrex discontinuous batch reactor with an external cooling jacket, enveloped by an aluminum foil and equipped with a UV 125 W Hg high pressure lamp, placed in a coaxial quartz cylinder. No optical filter was adopted. TiO_2 (100 ± 5 mg) was suspended by sonication in 400 ml of water containing 121 ± 2 ppm of phenol (PhOH) (93 ± 2 ppm as C). The temperature was kept 25 ± 2 °C. and the suspension was recirculated by a peristaltic pump (14 ml s^{-1}). pH and oxygen content were monitored by on-line sensors.

Photodegradation was performed in the presence of H_2O_2 or O_2 as oxidative agent. In the former experiment (homogeneous oxidation) stoichiometric amount of 35 wt% H_2O_2 aqueous solution was added (H_2O_2/PhOH = 14 mol/mol) and the suspension was circulated in the dark for 30 min before turning on the UV source. In the latter case (heterogeneous oxidation) the suspension was circulated in the dark and saturated in on-line chamber by continuously bubbling oxygen (100 ml min^{-1}); the excess of gas was eliminated through a non-return check valve. The UV source was turned on when the oxygen content in the suspension became maximum and constant (in about 10 min). The reaction was performed keeping constant the oxygen feed. In both cases control experiments were carried out in the absence of TiO_2 (blank experiments). In order to monitor the photoinduced degradation of phenol, aliquots (6 ml) of the reaction solution were drawn out at regular intervals. Then TiO_2 powder was separated by centrifuga-

Table 1
Phase composition, BET specific surface area and XRD particle size of hydrothermal TiO_2 samples.

	Phase composition		BET surface area (m^2 g^{-1})	XRD particle size	
	Anatase (wt%)	Rutile (wt%)		Anatase *d*(1 0 1) (nm)	Rutile *d*(1 1 0) (nm)
R100	0	100	22	–	53
R61	39	61	46	14	68
R57	43	57	60	15	31
R48	52	48	64	14	26
R20	80	20	68	16	35
R0	100	0	91	15	–

tion and the clear solution was analyzed for the TOC by using Shimadzu TOC-V CSH analyzer.

2.3. Electron paramagnetic resonance (EPR) measurements

The EPR investigation on the charge carrier species, O^-, Ti^{3+} and O_2^-, in UV irradiated TiO_2 samples, was performed by a Bruker EMX spectrometer working at the X-band frequency, equipped with an Oxford cryostat operating in the range of temperature 4–298 K. Spectra were recorded on powder samples under helium atmosphere at 10 K after 20 min of irradiation at this temperature inside the EPR cavity. The spectra were newly recorded 1 and 20 min after switching off the lamp. Modulation frequency was 100 kHz, modulation amplitude 3–10 gauss, microwave power 5–10 mW. For each sample, the absence of a signal before irradiation was checked. Irradiation was performed by UV 500 W Hg lamp (Jelosil, Italy), with the output radiation focused on the samples in the cavity by using an optical fiber (50 cm length, 1 cm diameter). Care was taken in order that the most sensitive part of the EPR cavity (1 cm length) was always filled.

The g values were calculated by standardization with α,α′-diphenyl-β-picryl hydrazyl (DPPH). The spin concentration was obtained by double integration of the resonance lines, referring the area to that of the standard Bruker weak pitch (9.7×10^{12} ± 5% spins cm^{-1}). Accuracy on double integration was ±20%. Spectra simulation and fit were performed by SIM 14S program [21].

2.4. Spin-trap EPR experiments

Spin-trap experiments were performed in order to determine the amount of the UV photogenerated short-living $OH^\bullet$ radicals in aqueous media. The measurements aimed to compare the photoactivity of selected hydrothermal TiO_2 catalysts in the PhOH oxidation with the number of $OH^\bullet$ radicals generated under similar reaction conditions, but in the absence of phenol. Spin-trap reagent was α-(4-pyridyl-1-oxide)-N-*tert*-butylnitrone (POBN).

The stock suspensions were prepared by dispersing TiO_2 in water (0.18 g/L) buffered at pH 7.0 (phosphate buffer), and carefully homogenizing in ultrasound bath (1 h). Then POBN (concentration 1.5×10^{-3} M) was added to the suspension. Buffered pH is necessary to avoid the absorption of spin trap molecules on TiO_2 surface; Bolton [20b] demonstrated that the relatively small effect of pH on $OH^\bullet$ formation do not preclude to significantly compare samples with different composition.

Two different procedures were applied to stock suspensions depending on the oxidative agent. In the case of H_2O_2, a suitable amount of 35 wt% H_2O_2 was added to the suspension in a reservoir, keeping the same concentration as in the phenol degradation experiments (0.210 g/L). Just a few minutes before irradiation, the solution was pumped into the EPR quartz flat cell (6 cm window length, 0.5 mm optical path) through a Teflon tube connected to the reservoir. In the case of O_2, the stock solution was purged before the experiment with pure O_2 for 1 h in the reservoir and then pumped into the EPR quartz flat cell.

EPR spectra were recorded at 293 K before and during the UV *in situ* irradiation. The irradiation source was a UV 500 W Hg lamp (Jelosil, Italy), with the output radiation focused on the cavity sample by using an optical fiber (50 cm length, 1 cm diameter). Typical EPR spectrometer settings were: microwave frequency: 9.8 GHz; microwave power: 10 mW; sweep width: 6–10 mT; modulation amplitude: 0.05–0.2 mT; scan time: 20.97–41.94; time constant: 40.96–81.92.

The maximum intensity of the first derivative peak of the spin-trapped paramagnetic adduct was plotted against reaction time in order to estimate the $OH^\bullet$ production in the irradiated suspensions. The initial slope r_0, calculated as tangent to the curve at the time when the adduct begins to form, was taken as representative parameter [20].

3. Results

3.1. Photocatalytic activity

The photocatalytic activity of the hydrothermal TiO_2 samples was measured in the phenol mineralization with H_2O_2 or O_2, under UV irradiation (see Section 2).

The catalytic tests were performed on a set of TiO_2 samples having wide range of phase composition (Table 1). Oxidative agents, whose chemical and physical properties are expected to influence in a different way the phenol degradation, were used: H_2O_2, which is water soluble and produces high amount of $OH^\bullet$ radicals [8], under UV irradiation in the presence of TiO_2 catalyst; O_2, which is partially soluble in water, but shows to be chemisorbed at the oxide surface as reduced species (e.g. superoxide O_2^-) [18,22,23]. Superoxide is further converted into $OH^\bullet$ radicals (see reactions (6)–(8)).

Fig. 1a and b shows the mineralization curves of phenol (given as TOC%) in the presence of some representative catalysts, using H_2O_2 and O_2, respectively. The maximum degradation rate $(dC/dt)_{max}$, which correspond to the maximum slope point of the fitted curves, and the half degradation time $t_{1/2}$, were taken as representative of the kinetic behavior of the different samples (Table 2). Both $(dC/dt)_{max}$ and $t_{1/2}$ values were calculated by reproducing the experimental data (TOC vs. time) with the function:

$$C(t) = C_0 - A\int_0^x \exp\left(-\frac{(t-t_0)^2}{s}\right) dt \quad (9)$$

Table 2
Photocatalytic parameters, number of photogenerated e^- and h^+ traps, $OH^\bullet$ formation rate in hydrothermal TiO_2 samples.

Samples	Photocatalytic parameters				Traps amount		$OH^\bullet$ formation rate[a]	
	H_2O_2		O_2		Ti^{3+} (spin/g)	O^- (spin/g)	H_2O_2	O_2
	$(dC/dt)_{max}$ (ppm/min)	$t_{1/2}$ (min)	$(dC/dt)_{max}$ (ppm/min)	$t_{1/2}$ (min)			Initial slope r_0	Initial slope r_0
R100	1.69	47	0.309[b]	470[b]	3.6E+18	8.8E+17	5.2E+04	3.9E+03
R61	1.40	46	0.512	147	1.4E+18	2.0E+17	1.4E+04	7.0E+03
R57	1.61	50	0.457	134			1.9E+04	7.4E+03
R48	1.32	50	0.487	107	1.1E+18	4.6E+17	2.1E+04	7.8E+03
R20	0.98	65	0.448	136	1.4E+18	2.3E+17	1.8E.+04	8.4E+03
R0	0.84	80	0,459	128	7.2E+16	1.1E+17	1.7E+04	8.8E+03
Blank	1.27	74	0.149[b]	740[b]			2.0E+04	2.9E+03

[a] Initial slope r_0 is the tangent to the curve of the EPR signal intensity of spin-trapped $OH^\bullet$ adduct vs. reaction time.
[b] Value extrapolated according to Eq (9).

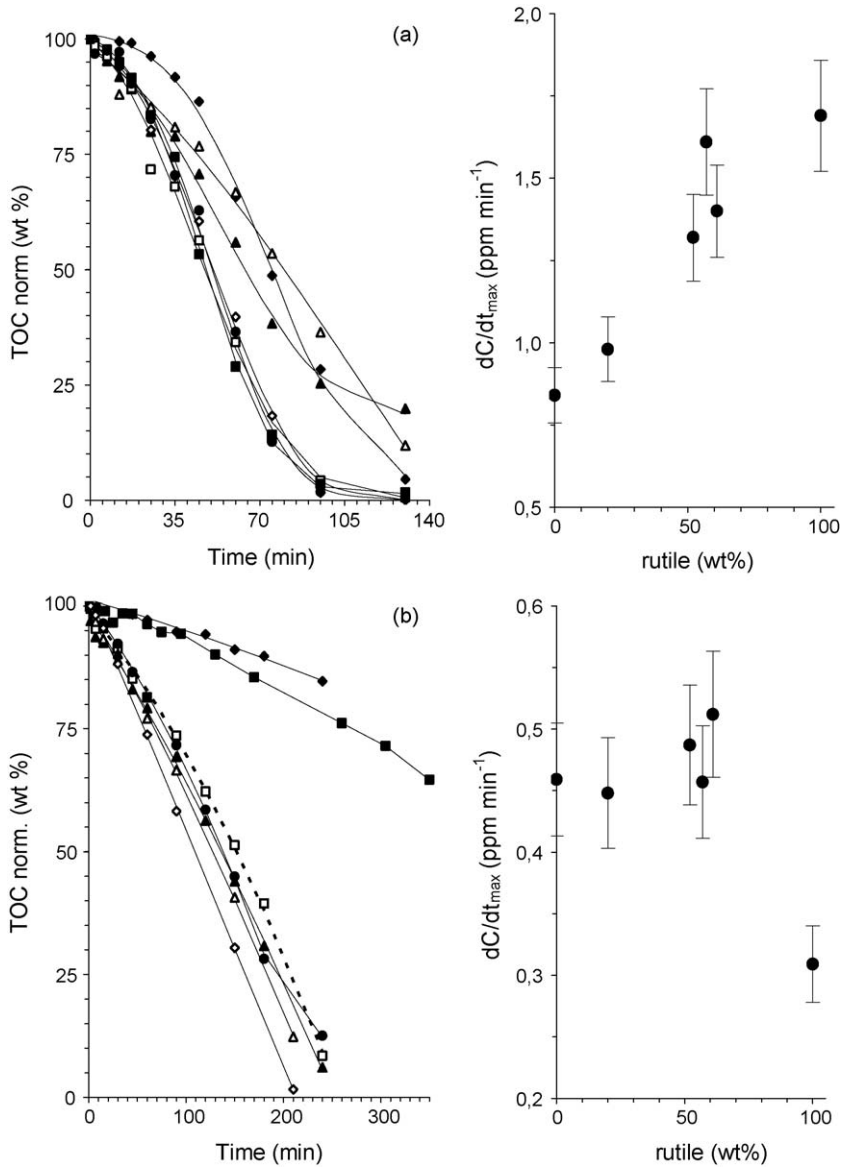

Fig. 1. Mineralization curves of phenol (given as TOC%) in the presence of some representative catalysts using (a) H_2O_2 and (b) O_2 as oxidative agents: (◆) blank; (■) R100; (□) R61; (●) R57; (◇) R48; (▲) R20; (△) R0. Dashed lines are the best fit to the experimental data according to Eq. (9). On the right the related plots of dC/dt_{max} vs. phase composition, expressed as rutile wt%, are reported.

where $C(t)$ is the TOC amount measured at the t time and C_0, A, t_0, s are fitting parameters (C_0 is the total organic carbon in solution before the phenol degradation and t_0 the time at which the mineralization of the organic substrate starts). The catalyst performances were evaluated after optimization of the fitting parameters (available in Supporting Information) and were normalized to the same mass (100 mg) of TiO_2.

When H_2O_2 is used as oxidizing agent, pure rutile shows the minimum value of $t_{1/2}$ and the maximum of $(dC/dt)_{max}$. On the other hand, pure anatase exhibits the lowest activity, slightly lower than the blank test performed in the absence of TiO_2. In mixed phase samples the photoactivity increases with the amount of rutile phase, though the relation between composition and activity is not strictly monotone (Fig. 1a).

If O_2 is the oxidizing agent, the photocatalytic activity is generally lower than in the case of H_2O_2. The values of $t_{1/2}$ decrease and those of $(dC/dt)_{max}$ increase in the samples containing anatase, while pure rutile shows the lowest photoactivity. These results indicate that the presence of anatase is essential to improve the activity in heterogeneous conditions. No significant differences were found between pure anatase and mixed phase samples (Fig. 1b). In the blank test, without the catalyst, the phenol mineralization rate is very low, thus indicating a minor contribution of direct phenol photolysis to the overall process.

Photoactivity parameters $t_{1/2}$ and $(dC/dt)_{max}$ were also calculated by normalizing them to surface area unit of catalyst. (The normalized plots of the maximum degradation rate $(dC/dt)_{max}$ vs. sample composition in the presence of H_2O_2 and O_2 are reported in Supporting Information). The results show that, in the presence of O_2, differences in surface area significantly influence the catalyst activity and confirm that, when using H_2O_2, the highest photoactivity is not related to the largest surface area.

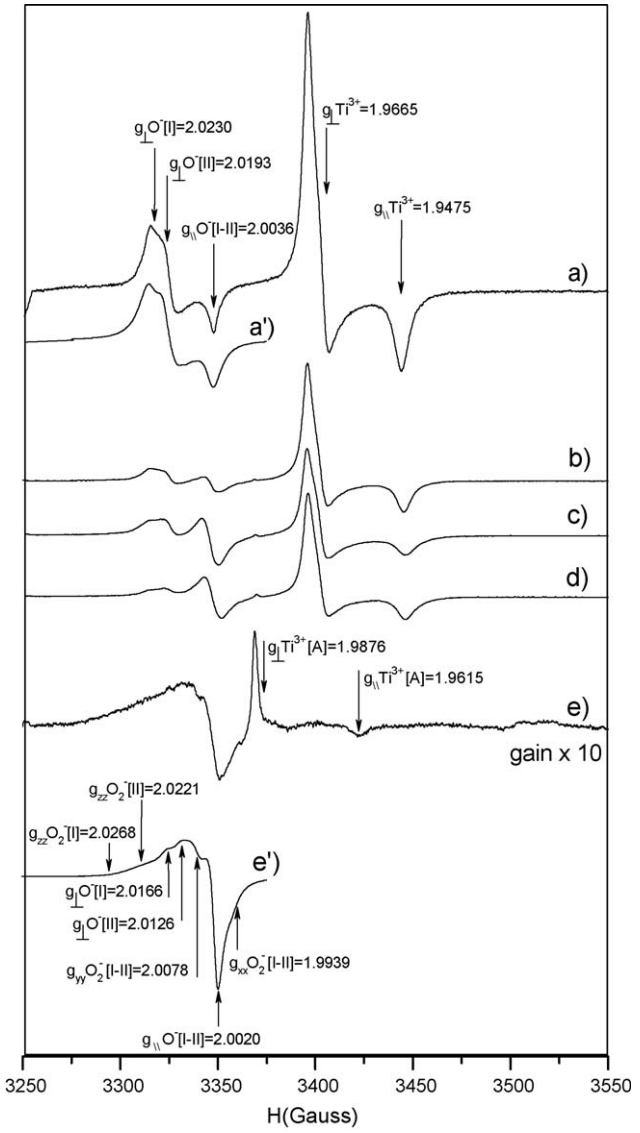

Fig. 2. EPR spectra of hydrothermal TiO_2 samples recorded at 10 K after 20 min of UV irradiation. (a) R100; (b) R61; (c) R48; (d) R20; (e) R0. (a′) and (e′) simulate (a) and (e) spectra, respectively.

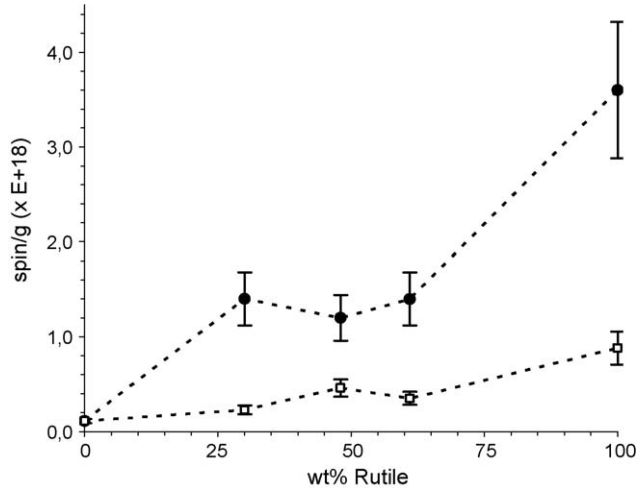

Fig. 3. Amount of paramagnetic (•) Ti^{3+} and (□) O^- after UV irradiation at 10 K vs. TiO_2 phase composition expressed as rutile wt%. Dotted lines are eye-guides.

3.2. Charge carrier characterization

Electron and hole traps centers, generated in hydrothermal TiO_2 by UV irradiation, were investigated by EPR, in order to relate the charge carrier lifetime to the catalyst efficacy.

Typical EPR spectra of pure anatase, pure rutile and of selected mixed phase samples, recorded after UV irradiation at 10 K, are shown in Fig. 2.

The higher field sharp signals at $g_\perp = 1.9665$ and $g_{||} = 1.9475$ in the spectra a–d of Fig. 2, are assigned to electrons trapped at Ti^{3+} sites of rutile ($Ti^{3+}_{[R]}$) [22,23,24a]. Their intensity is higher than that of the lower field resonances. The sharpness of Ti^{3+} resonance lines suggests crystalline environment of Ti^{3+} centers. In pure anatase the axial signals at $g_\perp = 1.9876$ and $g_{||} = 1.9615$ are assigned to electrons trapped at Ti^{3+} sites in the anatase lattice ($Ti^{3+}_{[A]}$) [22,23, 24a] (Fig. 2, spectrum e), but their intensity is much lower than that of Ti^{3+} resonances in rutile (Fig. 3). The lower field overlapped signals in pure rutile (Fig. 2, spectrum a′) were simulated and attributed to the resonances of holes trapped at two different O^- sites [22,24–26]: $O^-_{[R\text{-}I]}$ with $g_\perp = 2.0230$ and $g_{||} = 2.0036$ and $O^-_{[R\text{-}II]}$ with $g_\perp = 2.0193$ and $g_{||} = 2.0036$. The pure anatase lower field overlapped signals were attributed to two distinct O^- and two distinct O_2^- centers [21a,b,24]—$O^-_{[A\text{-}I]}$: $g_\perp = 2.0166$ and $g_{||} = 2.0020$ and $O^-_{[A\text{-}II]}$: $g_\perp = 2.0126$ and $g_{||} = 2.0020$; $O_2{}^-_{[A\text{-}I]}$: $g_{zz} = 2.0268$, $g_{yy} = 2.0078$, $g_{xx} = 1.9939$ and $O_2{}^-_{[A\text{-}II]}$: $g_{zz} = 2.0221$, $g_{yy} = 2.0078$, $g_{xx} = 1.9939$ (Fig. 2, spectrum e′). EPR spectra of mixed phase TiO_2 samples (Fig. 2, spectra b–d) show the signals of the two distinct $O^-_{[R\text{-}I]}$ and $O^-_{[R\text{-}II]}$ centers and of $Ti^{3+}_{[R]}$. They are very similar to those of pure rutile samples whatever the amount of anatase, showing that e^- and h^+ are preferentially trapped on the O^- and Ti^{3+} centers of rutile phase, even if anatase is the main component. This indicates that an electron transfer occurs from the higher energy conduction band states of anatase to those of rutile, lying at lower energy and, simultaneously, a hole transfer occurs from the lower energy valence band states of anatase to those of rutile lying at higher energy.

The number of O^- centers, is in the range 8.8×10^{17} spin g^{-1} (pure rutile)–1.1×10^{17} spin g^{-1} (pure anatase) while that of Ti^{3+} in the range 3.6×10^{18} spin g^{-1} (pure rutile)–1.1×10^{17} spin g^{-1} (pure anatase). The amount of both paramagnetic traps increases with the rutile content (Fig. 3).

In anatase, a small amount of superoxide O_2^- was observed although the UV irradiation was carried out under helium atmosphere. In the absence of oxygen, the formation of O_2^- may occur according to the scheme proposed by Grätzel [27], favored by the presence of hydroxyl groups:

$$2h^+ + 2OH^- \rightarrow 2OH^\bullet \rightarrow H_2O_2 \quad (10)$$

$$H_2O_2 + h^+ \rightarrow O_2^- + 2H^+ \quad (11)$$

The presence of O_2^- confirms the anatase attitude to chemisorb oxygen in a reduced form [8].

3.3. Spin-trapping experiments

Spin-trapping experiments allow to measure the short-lived reactive $OH^\bullet$ radicals produced in the presence of TiO_2, using H_2O_2 and O_2 as oxidative agents. The interaction of $OH^\bullet$ with the spin trapping reactant POBN yields the EPR active $^\bullet$POBN-OH

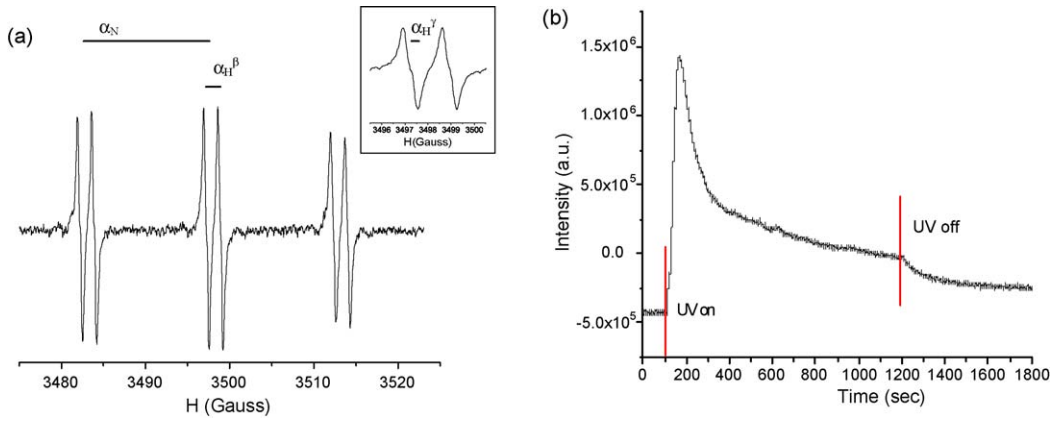

Fig. 4. (a) EPR spectrum of the •POBN-OH adduct. Hyperfine constants a_N, a_H^β and, in the inset, a_H^γ are indicated. (b) Typical variation of the intensity of •POBN-OH resonance lines with the irradiation time.

adduct in agreement to the reaction (rate constant $k = 3.8 \times 10^9\ M^{-1}\ s^{-1}$) [28]:

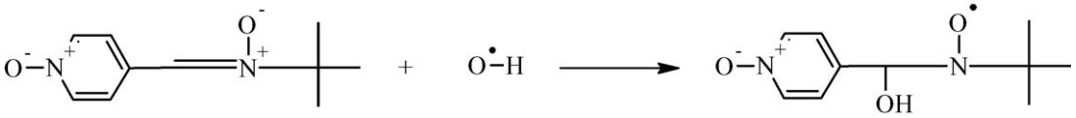

(12)

EPR spectra of the •POBN-OH adduct were recorded during the *in situ* UV irradiation (Fig. 4a). The EPR signal at $g = 2.0057$ is composed of 12 lines due to the hyperfine interaction with nitroxide, $a_N = 14.91$ gauss; to the interaction with the β-type H, $a_H^\beta = 1.699$, and with the γ-type H, a_H^γ 0.34 gauss [28]. The last one appears poorly resolved due to the line broadness (inset in Fig. 4a).

The intensity of •POBN-OH lines changes with the irradiation time, as shown by the typical curve reported in Fig. 4b. At the beginning of irradiation, the adduct rapidly forms and the signal intensity strongly increases with the time. The prolonged irradiation, however, results in a decrease of •POBN-OH concentration, probably due to multiple addition of hydroxyl radicals to POBN, leading to diamagnetic species, and/or to limited OH• production, due to the progressive oxidant (H_2O_2 or O_2) decrease in the EPR cell [19 c].

As a consequence, the maximum intensity of the EPR signal cannot be associated to the number of OH• radicals, or to the photocatalytic activity of TiO_2 samples. In order to compare the photoactivity of the different TiO_2 samples with the amount of OH• radicals, the most suitable and significant parameter is the initial slope r_0 in the curve of OH• intensity vs. time, corresponding to the initial rate of •POBN-OH formation.

The r_0 values of TiO_2 samples irradiated in the presence of H_2O_2 are plotted in Fig. 5a versus the wt% of rutile and compared with the blank test, in the absence of catalyst. Pure rutile shows the highest r_0 value, unlike pure anatase and mixed phase samples, which have behavior similar to that of the blank test. These results are in agreement with those of Hirakawa et al. [29], which attributed the increase of OH• formation to a specific coordination mode of H_2O_2 on rutile surface. This trend is generally respected also in our hydrothermal mixed phase samples, where the OH• generation slightly increases with the amount of rutile. The small differences between r_0 values are probably related to the presence of OH• radicals deriving from direct photolysis of H_2O_2 [30,31].

The r_0 values in TiO_2 samples, irradiated in the presence of O_2, are shown in Fig. 5b. As expected, the rate r_0 is generally lower than in the oxidation by H_2O_2. As a matter of fact OH• radicals cannot be produced by direct photolysis of H_2O_2 and result from reaction (2)

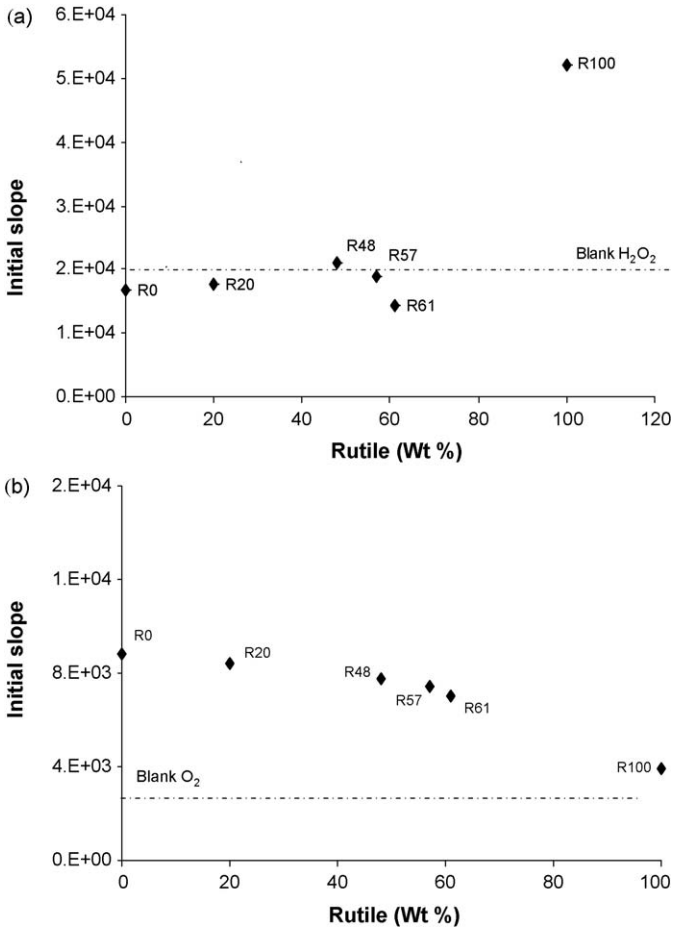

Fig. 5. Initial slope r_0 of •POBN-OH adduct formation under UV irradiation vs. phase composition expressed as rutile wt%, in the presence of (a) H_2O_2 and (b) O_2.

or from oxygen adsorption and reduction, reactions (5)–(8). The value of r_0 increases with the amount of anatase, while the lowest values were found for pure rutile samples.

In both the oxidative procedures (by H_2O_2 and O_2), r_0 values of mixed phase samples do not show strictly monotone dependence on the rutile amount.

4. Discussion and conclusions

The results reported in the present paper, concern with (i) the photoactivity of different-phase hydrothermal TiO_2 samples in the phenol oxidative degradation by H_2O_2 and O_2; (ii) the stabilization of electron and hole trap centers, Ti^{3+} and O^-, generated by UV irradiation of solid; (iii) the formation of hydroxyl radicals, $OH^\bullet$, in aqueous TiO_2 suspension in the presence of O_2 or H_2O_2.

Relationships may be found among the results of the experiments about the above topics. In fact:

(i) In agreement to what reported [6,7] in our previous papers on the same catalysts, if the oxidation is performed by H_2O_2, in homogeneous phase, pure rutile displays the highest catalytic efficiency, in comparison with mixed phase (anatase/rutile) samples. The very high catalytic activity of rutile is due to the lower tendency of electrons and holes to recombine in the large dimension crystalline rods of rutile, when compared to the smaller nanosized particles of anatase (5–15 nm).

When the process is performed in heterogeneous phase with gaseous O_2, the presence of anatase, both in pure and mixed phase, is essential to improve the photodegradation, while pure rutile displays the lowest catalytic activity. In fact, oxygen preferentially chemisorbs at the surface of anatase as O_2^- [8], acting as an effective electron scavenger. This extends the independent lifetime of electrons and holes, decreasing the electron–hole recombination rate even in small anatase particles and improving their photoactivity. Accordingly, photocatalytic parameters normalized to catalyst surface area unit show that, in the presence of O_2, the higher surface area of the small anatase particles positively affect their activity. Instead, differences in surface area and pore volume between samples do not explain the opposite trends of photocatalytic behaviors in the presence of H_2O_2, suggesting that the effects of crystal phase and particle size are dominant.

(ii) In accordance to the catalytic activity in the presence of H_2O_2, the high amount of photogenerated charge trapping centers, O^- and Ti^{3+}, in rutile rich samples, resulting from EPR measurements, together with the observed electron/hole transfer from anatase to rutile in mixed phase samples, confirm the stability of h^+ and e^- pairs in rutile.

(iii) The lifetime increase of the electron/hole pairs favors reactions (1)–(8) which ultimately produce the highly oxidant $OH^\bullet$ radicals, responsible for the phenol degradation. The relation between the $OH^\bullet$ radical formation rate, r_0 and the catalytic behavior clearly shows that hydroxyl radicals may be taken, at molecular level, as intermediate active species of the oxidation. In the case of oxidation by H_2O_2, the strict parallelism between r_0 and the crystalline phase becomes less evident in the mixed phase samples, due to the presence of $OH^\bullet$ produced by H_2O_2.

Acknowledgement

Authors thank the Cariplo Foundation for the financial support.

Appendix A. Supplementary data

Supplementary data associated with this article can be found, in the online version, at doi:10.1016/j.apcatb.2008.10.017.

References

[1] (a) M.R. Hoffmann, S.T. Martin, W. Choi, Chem. Rev. 95 (1995) 69–96;
(b) T.T. Thompson, J.T. Yates, Chem. Rev. 10 (2006) 4428–4453.
[2] A.L. Linsebigler, G. Lu, J.T. Yates Jr., Chem. Rev. 95 (1995) 735.
[3] (a) R.R. Bacsa, J. Kiwi, Appl. Catal. B 16 (1998) 19;
(b) S. Watson, D. Beydoun, J. Scott, R. Amal, J. Nanoparticle Res. 6 (2004) 193;
(c) M. Yan, F. Chen, J. Zhang, M. Anpo, J. Phys. Chem. B 109 (2005) 8673.
[4] (a) S.S. Watson, D. Beydoun, J.A. Scott, R. Amal, Chem. Eng. J. 95 (2003) 213;
(b) A. Mills, S.K. Lee, A. Lepre, J. Photochem. Photobiol. A 155 (2003) 199;
(c) M.H. Habibi, H. Vosooghian, J. Photochem. Photobiol. A 174 (2005) 45.
[5] (a) H. Fujii, M. Ohtaky, K. Eguchi, J. Am. Chem. Soc. 120 (1998) 6832;
(b) H. Yoshitake, T. Sugihara, T. Tatsumi, Chem. Mater. 14 (2002) 1023;
(c) D.M. Antonelli, Micropor. Mesopor. Mater. 30 (1999) 315;
(d) G.J.A.A. Soler-Illia, A. Louis, C. Sanchez, Chem. Mater. 14 (2002) 750;
(e) P. Yang, D. Zhao, D. Margolese, B.F. Chmelka, G.D. Stucky, Nature 396 (1998) 152;
(f) Y. Yue, Z. Gao, Chem. Commun. (2000) 1755;
(g) B. Tian, H. Yang, X. Liu, S. Xie, C. Yu, J. Fan, B. Tu, D. Zhao, Chem. Commun. (2002) 1824;
(h) P. Kluson, P. Kacer, T. Cajthaml, M. Kalaji, J. Mater. Chem. 11 (2001) 644;
(i) D. Grosso, G.J.A.A. Soler-Illia, E.L. Crepaldi, F. Cagnol, C. Sinturel, A. Bourgeois, A. Brunet-Bruneau, H. Amenitsch, P.A. Albouy, C. Sanchez, Chem. Mater. 15 (2003) 4562–4570;
(j) Y. Sakatani, D. Grosso, L. Nicole, G.J.A.A. Soler-Illia, C. Sanchez, J. Mater. Chem. 16 (2006) 77–82;
(k) E.L. Crepaldi, G.J.A.A. Soler-Illia, D. Grosso, F. Cagnol, F. Ribot, C. Sanchez, J. Am. Chem. Soc. 125 (2003) 9770–9786;
(l) H. Luo, C. Wang, Y. Yan, Chem. Mater. 15 (2003) 3841–3846;
(m) C. Sanchez, C. Boissiere, D. Grosso, C. Laberty, L. Nicole, Chem. Mater. 20 (2008) 682–737;
(n) E. Martinez-Ferrero, Y. Sakatani, C. Boissiere, D. Grosso, A. Fuertes, J. Fraxedas, C. Sanchez, Adv. Funct. Mater. 17 (2007) 3348–3354.
[6] A. Testino, I.R. Bellobono, V. Buscaglia, C. Canevali, M. D'Arienzo, S. Polizzi, R. Scotti, F. Morazzoni, J. Am. Chem. Soc. 129 (2007) 3564–3575.
[7] R. Scotti, I.R. Bellobono, C. Canevali, C. Cannas, M. Catti, M. D'Arienzo, A. Musinu, S. Polizzi, M. Sommariva, A. Testino, F. Morazzoni, Chem. Mater. 20 (2008) 4051–4061.
[8] A. Sclafani, J.M. Herrmann, J. Phys. Chem. 100 (1996) 13655.
[9] P. Salvador, J. Phys. Chem. C 111 (2007) 17038.
[10] U. Diebold, Surf. Sci. Rep. 48 (2003) 53.
[11] P. Davit, G. Martra, S. Coluccia, Jpn. Petr. Institut. 47 (2004) 359.
[12] G.V. Buxton, C.L. Greenstock, W.P. Helman, A.B. Ross, J. Phys. Chem. Ref. Data 17 (2) (1988) p516.
[13] J. Theurich, M. Lindner, D.W. Bahnemann, Langmuir 12 (1996) 6368.
[14] R. Vinu, G. Madras, Environ. Sci. Technol. 42 (2008) 913.
[15] M. Ampo, T. Shima, Y. Kubokawa, Chem. Lett. 12 (1985) 1799.
[16] K. Okamoto, Y. Yakamoto, H. Tanaka, M. Tanaka, M.A. Itaya, Bull. Chem. Soc. Jpn. 58 (1985) 2015.
[17] I. Illisz, A. Dombi, Appl. Catal. A 180 (1999) 35.
[18] T. Hirakawa, T. Daimon, M. Kitazawa, N. Ohguri, C. Koga, N. Negishi, S. Matsuzawa, Y. Nosaka, J. Photochem. Photobiol. A: Chem. 190 (2007) 58.
[19] (a) V. Brezova, A. Staško, S. Biskupič, A. Blažkova, B. Havlinova, J. Phys. Chem. 98 (1994) 8977–8984;
(b) V. Brezova, S. Gabčova, D. Dvoranova, A. Staško, J. Photochem. Photobiol. B 79 (2005) 121–134;
(c) V. Brezova, D. Dvoranova, A. Staško, Res. Chem. Intermed. 33 (2007) 251–268.
[20] (a) J. Kochany, J.R. Bolton, J. Phys. Chem. 95 (1991) 5116–5120;
(b) G. Riegel, J.R. Bolton, J. Phys. Chem. 99 (1995) 4215–4224.
[21] G.P. Lozos, B.M. Hofman, C.G. Franz, Quantum Chemistry Program Exchange, no. 65, 1973.
[22] (a) T. Berger, M. Sterrer, O. Diwald, E. Knözinger, ChemPhysChem 6 (2005) 2104–2112;
(b) T. Berger, M. Sterrer, O. Diwald, E. Knözinger, D. Panayotov, T.L. Thompson, J.T. Yates Jr., J. Phys. Chem. B 109 (2005) 6061–6068;
(c) J.E. Elser, T. Berger, M. Sterrer, D. Brandhuber, J. Bernardi, O. Diwald, E. Knözinger, J. Phys. Chem. B 110 (2006) 7605–7608;
(d) T. Berger, O. Diwald, E. Knözinger, M. Sterrer, J.T. Yates Jr., Phys. Chem. Chem. Phys. 8 (2006) 1822–1826.
[23] (a) D.C. Hurum, A.G. Agrios, K.A. Gray, T. Rajh, M.C. Thurnauer, J. Phys. Chem. B 10 (2003) 4545–4549;
(b) D.C. Hurum, K.A. Gray, T. Rajh, M.C. Thurnauer, J. Phys. Chem. B 109 (2005) 977–980;
(c) D.C. Hurum, A.G. Agrios, S.E. Crist, K.A. Gray, T. Rajh, M.C. Thurnauer, J. Electr. Spectr. 10 (2006) 155–163.

[24] (a) C.P. Kumar, N.O. Gopal, T.C. Wang, M.S. Wong, S.C. Ke, J. Phys. Chem. B 110 (2006) 5223–5229;
(b) S.C. Ke, T.C. Wang, M.S. Wong, N.O. Gopal, J. Phys. Chem. B 110 (2006) 11628–11634;
(c) J.M. Coronado, A.J. Maira, C.J. Conesa, K.L. Yeung, V. Augugliaro, J. Soria, Langmuir 17 (2001) 5368–5374;
(d) K.L. Yeung, S.T. Yau, A.J. Maira, J.M. Coronado, J. Soria, P.L. Yue, J. Catal. 17 (2003) 107–116;
(e) J.M. Coronado, J. Soria, J. Catal. Today 123 (2007) 37–41.
[25] (a) A.L. Attwood, D.M. Murphy, J.L. Edwards, T.A. Egerton, R.W. Harrison, Res. Chem. Intermed. 29 (2003) 449–465;
(b) E. Carter, A.F. Carley, D.M. Murphy, J. Phys. Chem. C 11 (2007) 10630–10638.
[26] M. Che, A.J. Tench, Adv. Catal. 31 (1982) 77.
[27] R.F. Howe, M. Grätzel, J. Phys. Chem. 91 (1987) 3906–3909.
[28] E.G. Janze, Y.Y. Wang, R.V. Shetty, J. Am. Chem. Soc. 100 (1978) 2923–2925.
[29] T. Hirakawa, K. Yawata, Y. Nosaka, Appl. Catal. A 325 (2007) 105–111.
[30] E. Selli, I.R. Bellobono, M.L. Raimondi, Angew. Makromol. Chem. 196 (1992) 169.
[31] J.H. Baxendale, J.A. Wilson, Trans. Faraday Soc. 53 (1957) 344.